JACS
JOURNAL OF THE AMERICAN CHEMICAL SOCIETY
Article
pubs.acs.org/JACS

Imaging the Evolution of *d* States at a Strontium Titanate Surface

Ikutaro Hamada,*[,†,‡,¶] Ryota Shimizu,[†,¶] Takeo Ohsawa,[†,§] Katsuya Iwaya,[†,∥] Tomihiro Hashizume,[†,⊥,#] Masaru Tsukada,[†] Kazuto Akagi,[†] and Taro Hitosugi*[,†,∇]

[†]Advanced Institute for Materials Research (AIMR), Tohoku University, Sendai 980-8577, Japan
[‡]International Center for Materials Nanoarchitectonics (MANA), and [§]Optical and Electronic Materials Unit, National Institute for Materials Science, Tsukuba 305-0044, Japan
[∥]RIKEN Center for Emergent Matter Science, Wako 351-0198, Japan
[⊥]Central Research Laboratory, Hitachi, Ltd., Saitama 350-0395, Japan
[#]Department of Physics, Tokyo Institute of Technology, Tokyo 152-8551, Japan
[∇]PRESTO, Japan Science and Technology Agency, Tokyo 102-0076, Japan

Supporting Information

ABSTRACT: Oxide electronics is a promising alternative to the conventional silicon-based semiconductor technology, owing to the rich functionalities of oxide thin films and heterostructures. In contrast to the silicon surface, however, the electronic structure of the $SrTiO_3$ surface, the most important substrate for oxide thin films growth, is not yet completely understood. Here we report on the electronic states of a reconstructed (001) surface of $SrTiO_3$ determined in real space, with scanning tunneling microscopy/spectroscopy and density functional theory calculations. We found a remarkable energy dependence of the spectroscopic image: Theoretical analysis reveals that symmetry breaking at the surface lifts the degeneracy in the t_{2g} state (d_{xy}, d_{yz}, and d_{zx}) of Ti 3*d* orbitals, whose anisotropic spatial distribution leads to a sharp transition in the spectroscopic image as a function of energy. The knowledge obtained here could be used to gain further insights into emergent phenomena at the surfaces and interfaces with $SrTiO_3$.

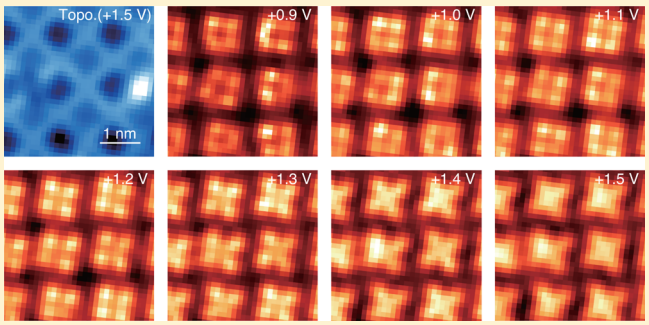

INTRODUCTION

Strontium titanate ($SrTiO_3$) is an archetypical oxide with the perovskite structure, which exhibits a rich variety of phenomena such as metal−insulator transition,[1] superconductivity,[2] and quantum paraelectricity.[3] Aside from the bulk properties, interfaces formed with the $SrTiO_3$ (001) surface have attracted enormous attention, since the discovery of the two-dimensional electron gas at the $LaAlO_3/SrTiO_3$ interface.[4] This was later shown to exhibit various intriguing properties, including magnetism,[5,6] superconductivity,[7] and large negative magnetoresistance.[8] The surface of $SrTiO_3$ has also attracted attention in its own right, because of the fascinating properties such as photocatalysis[9,10] and two-dimensional electron gas (liquid) on the surface.[11,12] Furthermore, $SrTiO_3$ is an important substrate for oxide thin film growth. To fabricate high quality oxide thin films and heterointerfaces in a controlled fashion, precise knowledge of the surface electronic properties is essential. However, owing to the structural complexity and highly defective nature of oxides, understanding the electronic structure of the $SrTiO_3$ surface at the atomic scale remains a formidable task. In recent works,[13] we revealed that the $SrTiO_3$ (001) surface with a step/terrace structure, prepared with a widely used BHF etching technique,[14] is atomically disordered despite the observation of streaky reflection high-energy electron diffraction (RHEED) patterns. It should be stressed here that the streak observed in the RHEED pattern does not guarantee a perfect atomically ordered surface.[15−17] Consequently, a straightforward and experimentally feasible solution is to use a reconstructed surface for the surface studies and for the substrate of epitaxial thin films. Among a variety of reported reconstructed $SrTiO_3$ surfaces (see ref 18 for a review), a $(\sqrt{13} \times \sqrt{13})$-*R*33.7° (hereafter referred to as $(\sqrt{13} \times \sqrt{13})$ for brevity) reconstructed surface is of particular interest, since the structure is reproducible,[19] and quite stable under an ambient condition,[20] as well as a wide range of conditions for thin film deposition, even after heating at 1000 °C in an oxygen partial pressure of 1×10^{-2} Torr.[13,19] For this $(\sqrt{13} \times \sqrt{13})$ reconstructed surface, Kienzle et al.[21] proposed an atomic arrangement based on the TiO_2 double layer[22] using transmission electron diffraction (TED) along with total energy calculations based on density functional theory (DFT). They also showed that the calculated surface energy of this $(\sqrt{13} \times \sqrt{13})$ reconstructed surface is the lowest among several TiO_2

Received: September 7, 2014
Published: November 27, 2014

   dx.doi.org/10.1021/ja509231w | J. Am. Chem. Soc. 2014, 136, 17201−17206

double layer based reconstructed surfaces.[21] However, the understanding of the surface electronic structure near the Fermi level, which is essential to the investigation of electron conductivity and magnetism, is far from satisfactory.

In this Article, we report on the atomic and electronic structures of $SrTiO_3$ (001) ($\sqrt{13} \times \sqrt{13}$) surface, using high resolution scanning tunneling microscopy (STM) and spectroscopy (STS) images acquired at low temperature, and DFT. STM combined with DFT has been used to study the reconstructed $SrTiO_3$ (001)[23−27] as well as (110)[28,29] surfaces, but to date energy-resolved STS mapping of the $SrTiO_3$ surface, which provides direct information on the surface electronic states in real space, has not yet been performed. We deduced an atomic structure of the $SrTiO_3$ (001) ($\sqrt{13} \times \sqrt{13}$) reconstructed surface from STM image analysis and DFT calculations, which agrees well with that proposed by Kienzle et al.[21] Moreover, we performed energy-resolved STS mapping and visualized the spatial distribution of the surface Ti 3*d* states, which shows a significant energy dependence. Based on the DFT analysis, we revealed that the interplay between the electronic states and the lattice degrees of freedom leads to the remarkable energy dependence of the STS image.

METHODS

As-supplied Nb-doped (0.1 atom %) $SrTiO_3$ (001) single crystals (Shinkosha Co., Ltd.) were used to ensure conductivity for low-temperature STM/STS measurements. An atomically ordered reconstructed surface with step and terrace structures was prepared at the temperature of 850 °C for 40 min at an oxygen pressure of 10^{-5} Torr, flushing at 1000 °C for a few minutes.[13,19] Ar^+ sputtering was not employed, because ion bombardment damages caused by the sputtering process lead to a large deviation from the stoichiometric condition, which would induce several surface reconstructions.[26] After preparation, the sample was immediately transferred to an UHV-STM system without exposure to air.[30] All the STM measurements were performed at 5 K. In STS measurements, the tunneling conductance spectra were obtained from numerical differentiation of the tunneling current (I) at each point, as a function of the sample bias voltage (V). Normalized differential conductance is defined by $(dI/dV)/(I/V) = d(\ln I)/d(\ln V)$.

All our DFT calculations were performed with a plane-wave basis set and ultrasoft pseudopotentials[31] within the Wu−Cohen[32] generalized gradient approximation (GGA), as implemented in the STATE[33] code. The surface was modeled by using a three-SrO layer slab with the bottom surface terminated by SrO. The slab was constructed using the theoretically optimized lattice constant of 3.909 Å, which is 0.5 (0.1) % larger than the experimental value of 3.89[34] (3.905[35]) Å. The slabs are separated by a vacuum equivalent to 4.5 SrO−TiO_2 bilayer (9 monolayer) thickness (~17.7 Å), and artificial electrostatic interaction with image slabs[36] was eliminated by using the effective screening medium method.[37] The atoms in the bottom SrO layer were fixed at their respective bulk positions, and remaining degrees of freedom are relaxed until the forces acting on them are small than 0.05 eV/Å. We used cutoff energies of 25 and 225 Ry for wave functions and augmentation charge, respectively, and the Γ-point approximation was adopted for Brillouin zone integration. STM images were simulated based on the Tersoff−Hamann[38] theory, and a Γ-centered 6 × 6 *k*-point set was used for the STM simulations. It has been shown[39,40] that the relative energy levels of unoccupied electronic states near the conduction band minimum within DFT are in good agreement with those obtained using the many-body GW approximation, despite the DFT error in the band gap.

RESULTS AND DISCUSSION

Figure 1a displays a topographic STM image of the $SrTiO_3$ (001) ($\sqrt{13} \times \sqrt{13}$) reconstructed surface, acquired at the

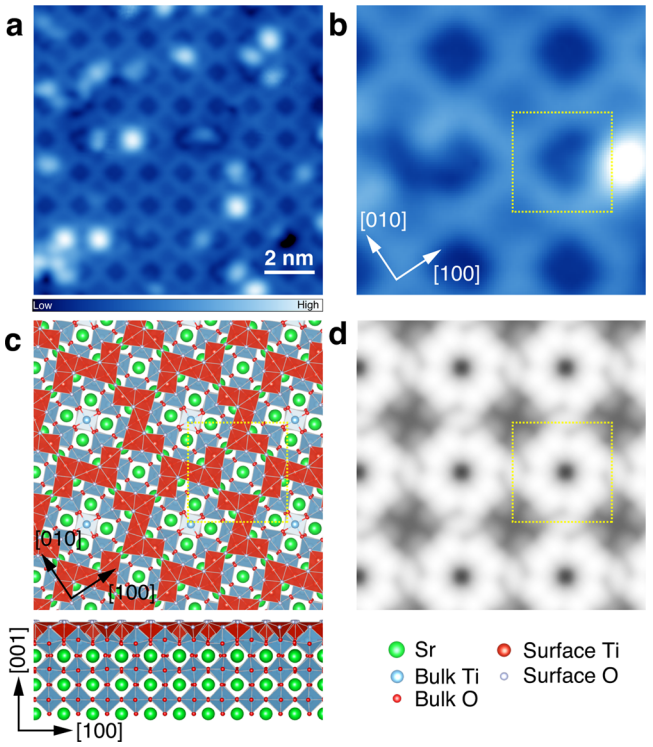

Figure 1. (a) Topographic STM image of $SrTiO_3$ (001) ($\sqrt{13} \times \sqrt{13}$)-*R*33.7° at the sample bias voltage (V_s) of +1.5 V and tunneling current of 30 pA (11.5 × 11.5 nm^2). (b) Magnified image (3.7 × 3.7 nm^2). (c) Surface structure determined from the high resolution STM image and DFT modeling. (d) Simulated STM topography at V_s = +1.5 V. Sample bias is referred to the conduction band minimum. Blue and red polyhedra in (c) indicate TiO_6 octahedra in bulk and truncated octahedra TiO_5 at the surface, respectively. The dotted squares in (b)−(d) indicate the ($\sqrt{13} \times \sqrt{13}$) surface unit cell.

sample bias voltage (V_s) of +1.5 V (unoccupied states), which shows a checkerboard pattern with a ($\sqrt{13} \times \sqrt{13}$) periodicity and 4-fold symmetry [see the magnified image, Figure 1b]. We note that observed bright spots are presumably associated with oxygen vacancies or adsorbed hydroxyl groups caused by a small amount of water, as the density of the bright spots depends on the oxygen partial pressure.[41] In the following, we focus on the defect free surface.

To determine the structure of the $SrTiO_3$ (001) ($\sqrt{13} \times \sqrt{13}$) reconstructed surface, we performed the surface modeling based on the high resolution STM image as follows: By inspecting the STM topography, we found that the checkerboard pattern consists of two types of tiles, that is, dark and faint-dark ones, separated by the bright lattice (Figure 1a and b). We assigned the dark tiles to vacant sites in the TiO_x adlayer on the bulklike TiO_2 terminated surface (similar to the TiO_2 double layer model), because our calculations showed that the bright/dark contrast could be reproduced by a combination of TiO_x adlayer (bright) and bulklike TiO_2-terminated subsurface (dark). Then, a TiO_x adlayer was constructed to satisfy the observed periodicity and the 4-fold symmetry. These constraints significantly reduced the number of possible arrangements of the TiO_x adlayer. Finally, the numbers and sites for O atoms were uniquely determined by assuming the stoichiometric composition of the adlayer (TiO_2) within our modeling (see the Supporting Information for details). The atomic structure was fully optimized with DFT, and the simulated STM topography was compared with the

dx.doi.org/10.1021/ja509231w | J. Am. Chem. Soc. 2014, 136, 17201−17206

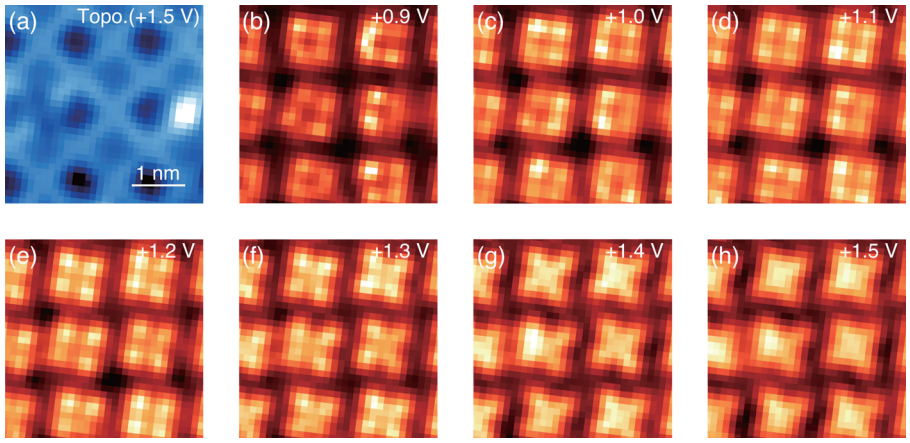

Figure 2. (a) STM topography at V_s = +1.5 V simultaneously acquired during the STS measurement (32 × 32 pixels in a 3.5 × 3.5 nm^2). (b–h) dI/dV images for V_s from +0.9 V to +1.5 V. Feedback set points are V_s = +1.5 V, I_t = 30 pA. The I–V curves were acquired at each point from +1.5 to −3.5 V with an energy resolution of 9.8 meV, and then numerically differentiated with a smoothing process to obtain the dI/dV images. Note that the data shown here are rotated by about 10° to compare with the simulated images.

experiment. We calculated formation energy for the surface oxygen vacancy using the experimental O_2 binding energy to correct for the DFT error, to obtain 4.9 eV/O relative to the gas-phase O_2 molecule, suggesting that the stoichiometric TiO_2 adlayer is favorable.

The structure thus determined is displayed in Figure 1c. A stoichiometric TiO_2 layer is formed on the bulklike TiO_2 terminated surface, which consists of truncated octahedra (TiO_5) stabilized by sharing their edges with the TiO_6 octahedra underneath. The Z-shaped framework composed of edge sharing five TiO_5 units forms a two-dimensional network by connecting to the corner of the TiO_5, which can be considered as a TiO_2 adlayer with small and large vacant sites. The calculated electronic structure indicates that the surface is insulating (as expected from the stoichiometric surface composition) with an energy gap of ∼2.0 eV, consistent with the tunneling spectroscopy, in which no in-gap states were observed (Supporting Information Figure S2). Thus, the oxidation state of the surface Ti is 4+, in line with the X-ray photoemission spectroscopy measurements.[19] Our simulated STM image (Figure 1d) is in qualitative agreement with the experiment, reproducing the features such as bright lattice, dark and faint dark tiles in the checkerboard pattern. Essentially, the STM allows visualization of the Ti atoms in the topmost TiO_2 adlayer, as the Ti 3*d* states have large contribution to the local density of states (charge density) for the unoccupied states. This is similar to what was found for the double layer TiO_2 (2 × 1) reconstructed $SrTiO_3$ (001) surface.[24] However, upon closer inspection the area of the dark tiles (width of the bright lattice) in the simulated image is much smaller (larger) than that of the experimental one. We presume the disagreement is mainly because of the absence of the tip electronic structure in our STM simulation. Taking the tip effect into consideration has been shown to significantly improve the agreement between the experimental and simulated STM images of rutile TiO_2(110).[42] The surface structure presented in this work coincides with the one proposed by Kienzle et al.[21] using TED and DFT calculations, despite the different sample preparation conditions, suggesting the stability and reproducibility of the $(\sqrt{13} \times \sqrt{13})$ reconstructed surface.

To investigate the surface electronic structures, we performed STS mapping for various sample biases. Figure 2 displays the normalized differential conductance (hereafter referred to as dI/dV for brevity) maps at various V_s. At V_s = +0.9 V (Figure 2b), a rounded square (squircle) shaped pattern was observed. Counterintuitively, the centers of the bright portions in the dI/dV map are located at the positions for the dark tiles in the STM topography (small vacant sites in the TiO_2 adlayer). The bright squares are tilted slightly, becoming brighter as V_s is increased (Figure 2c). At V_s = +1.1 V, the "dots" at the corners of squares are pronounced (Figure 2d), and become brighter by increasing V_s (Figure 2e). Eventually, the image shows a transition into a four lobe shaped pattern at V_s = +1.3 V (Figure 2f-h), suggesting a significant change in the observed surface electronic state.

We simulated the STS maps by calculating the spatially resolved local density of states (LDOS). Our simulated images are depicted in Figure 3a–c. At a lower bias, a rounded square shape pattern is formed, and the tilt of the squares changes with increasing the sample bias (Figure 3a,b). The pattern changes

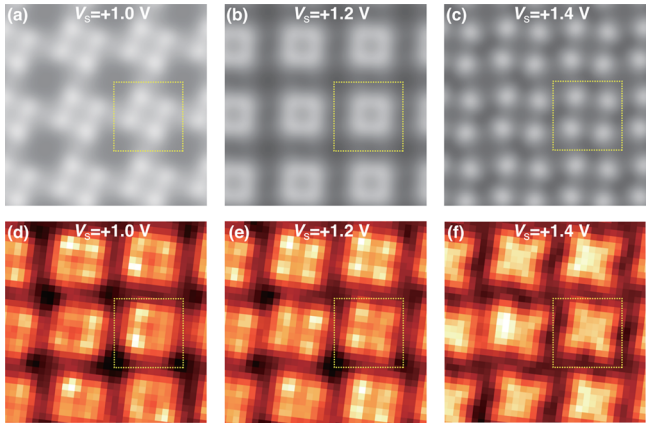

Figure 3. (a–c) Simulated dI/dV (LDOS) images at V_s = +1.0, +1.2, and +1.4 V, respectively. (d–f) The corresponding experimental dI/dV images. The size of the images are the same as those in Figure 2. Dotted squares indicate the $(\sqrt{13} \times \sqrt{13})$ surface unit cell and the positions are the same as those in Figure 1b–d. Simulated images were taken at 1.0 nm relative to the topmost surface composed of O atoms. The overall character of the simulated image was unchanged when computed at different height (Supporting Information Figure S3).

dx.doi.org/10.1021/ja509231w | J. Am. Chem. Soc. 2014, 136, 17201–17206

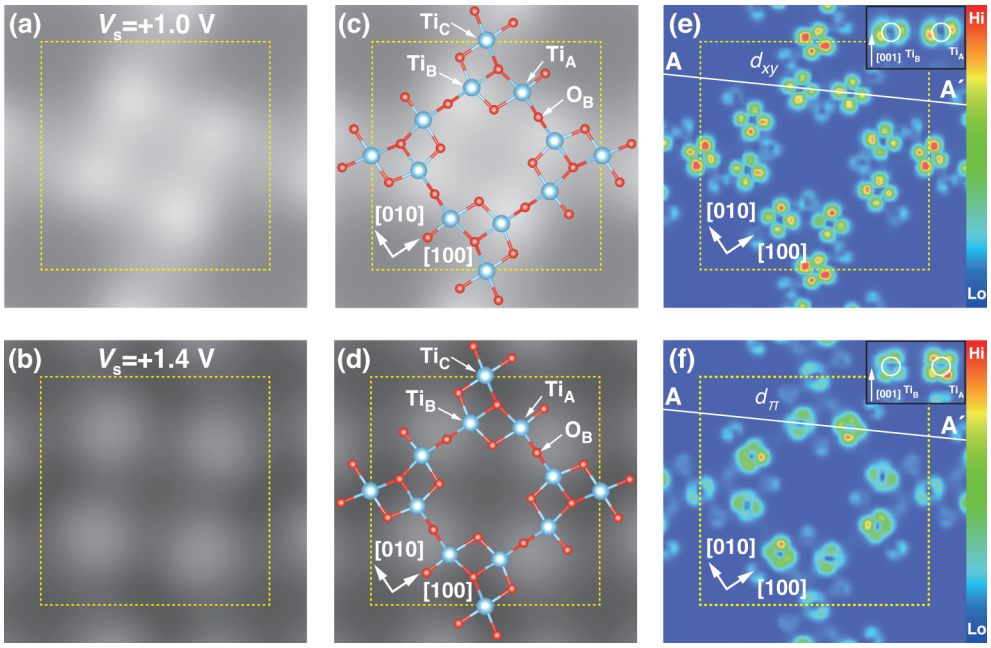

Figure 4. Simulated dI/dV images of $SrTiO_3$ (001) ($\sqrt{13} \times \sqrt{13}$) at V_s = +1.0 V (a) and +1.4 V (b). Those at V_s = +1.0 V (c) and +1.4 V (d), with the TiO_2 adlayer overlaid. Two dimensional plot of LDOS in the plane containing the TiO_2 adlayer at V_s = +1.0 V (e) and +1.4 V (f). In the insets of (e) and (f), LDOSs in the vicinity of Ti_A and Ti_B projected on the plane indicated by A–A′ are shown. Dotted squares indicate the surface unit cell, and their positions are the same as those in Figures 1 and 2.

from a square into a four lobe one at higher bias (Figure 3c), in qualitative agreement with the experimental dI/dV maps. There is non-negligible LDOS at the center of the lobe structure, which becomes visible by changing the tip height in the simulation (Supporting Information Figure. S3). Although the agreement between experimental and simulated images at lower bias is less satisfactory (in particular, there is an inverse correspondence at V_s = +1.0 V and +1.2 V), the transition from rounded square to four lobe patterns is nicely reproduced, validating the surface electronic states obtained from DFT calculations. It is noted that the tilt angle of the rounded square observed at a lower bias (V_s = +1.0 V and +1.2 V) is determined by a subtle balance of the decay length for Ti d_{xy} orbitals, and thus, for the quantitative simulation of the STS image, very accurate description of atomic positions (heights of Ti atoms), energy levels, and wave function tails is required. Nevertheless, an STS image at a lower bias is dominated by Ti d_{xy} and our conclusion is unchanged if we use advanced electronic structure method.

To understand the remarkable energy dependence of dI/dV, we analyzed the calculated electronic structures in detail. Figure 4 displays magnified dI/dV maps simulated at V_s = +1.0 V (rounded square, a) and +1.4 V (four-lobe, b). The wave functions (LDOSs) are centered at the surface Ti sites and distributed broadly into the smaller vacant sites of the TiO_2 adlayer at V_s = +1.0 V (Figure 4c), while they are localized in the vicinity of the corner sharing O sites (O_B) of TiO_5 at V_s = +1.4 V (Figure 4d). By inspecting the spatial distribution of LDOS at the surface (Figure 4e,f) and the density of states (Figure 5), we found that the t_{2g} states of the 3d orbitals for surface Ti atoms are imaged in the dI/dV maps. The t_{2g} states (d_{xy}, d_{yz}, and d_{zx}) form the conduction band minimum of bulk cubic $SrTiO_3$, and its degeneracy lifts upon formation of the (reconstructed) surface (see Supporting Information Figure S4 for a schematic energy diagram). There are nonequivalent Ti atoms in the surface TiO_2 adlayer (Ti_A, Ti_B, and Ti_C), which

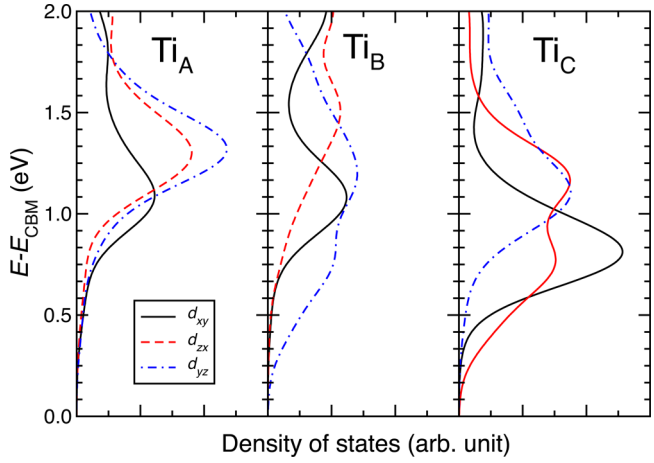

Figure 5. Density of states projected onto the d orbitals (xy, yz, and zx) of nonequivalent surface Ti atoms for $SrTiO_3$ (001) ($\sqrt{13} \times \sqrt{13}$). See Figure 4 for the notation of Ti atoms.The origin of the energy is set to the conduction band minimum (E_{CBM}).

have different oxygen coordination geometries [Figure 4c and d]: For instance, Ti_A and Ti_B have corner sharing O atoms (O_B) in addition to edge sharing O atoms, while the TiO_5 unit composed of Ti_C has edge sharing O atoms only. Thus, the energy levels and localizations of the orbitals for these Ti atoms are different. At V_s = +1.0 V, the d_{xy} orbitals of surface Ti atoms, which are distributed laterally, dominate the surface electronic states (Figure 4e). The d_{xy} orbital for Ti_C is more localized and has a larger density of states (Figure 5), decaying rapidly, while those for Ti_A and Ti_B are delocalized and have long-range decay in the vacuum region. As a result of the different decay lengths, the broad squircle shaped structure with brighter contrast at the Ti_A and Ti_B sites is imaged (Ti_B is slightly brighter, because its d_{xy} orbital is more delocalized). On the other hand, linear combinations of d_{yz} and d_{zx} orbitals (d_π) of Ti_A and Ti_B become

dx.doi.org/10.1021/ja509231w | J. Am. Chem. Soc. 2014, 136, 17201–17206

dominant at V_s = +1.4 V (Figure 4f). The d_π orbitals for Ti_C are localized and decay rapidly in space, while the lobes of those orbitals for Ti_A and Ti_B are distributed in the surface normal direction (diagonal directions of the Ti−O bonds in the TiO_5 units, inset of Figure 4f) and have long-range decay, resulting in bright portions localized in the vicinity of O_B. Taken together, the energy dependence of the spectroscopic image observed is attributed to the change in the *d* orbitals probed with STM, that is, d_{xy} at lower bias ($\lesssim$ +1.2 V) and d_π at higher bias ($\gtrsim$ + 1.3 V). Our DFT analysis revealed that the evolution of the d*I*/d*V* image is a consequence of the anisotropic nature of the *d* orbitals and complex surface structure, and that the splitting of the Ti *d* levels leads to the significant change in the spectroscopic image.

SUMMARY AND OUTLOOK

We have presented the atomic and electronic structures of the atomically ordered $SrTiO_3$ (001) $(\sqrt{13} \times \sqrt{13})$-*R*33.7° reconstructed surface, as revealed by the combination of high-resolution STM/STS imaging and DFT modeling. The Ti 3*d* t_{2g} states and their splitting caused by the symmetry breaking at the surface presented here have direct implications for the hererointerfaces formed with $SrTiO_3$. It has been suggested that the split Ti 3*d* t_{2g} orbitals, in particular, the Ti 3d_{xy} orbital, plays the decisive role in the interface conductivity and ferromagnetism at the $LaAlO_3/SrTiO_3$ interface,[43−45] and the present work visualizes how these 3*d* orbitals distribute in real space. The well-defined surface presented here would provide an opportunity to investigate chemical processes with atomic resolution toward understanding the mechanisms of growth chemistry[13,41] and catalytic reactions on the complex oxide surface.[46] Moreover, by combining its inherent nanoscale structure with functional oxide materials, the $SrTiO_3$(001) $(\sqrt{13} \times \sqrt{13})$-*R*33.7° reconstructed surface may pave the way to the novel *nano*-oxide electronics and spintronics.

ASSOCIATED CONTENT

Supporting Information

Details of the computational method and surface modeling, average d*I*/d*V* spectrum, height dependence of the simulated d*I*/d*V* images, and electronic structure for the $SrTiO_3$ (001) $(\sqrt{13} \times \sqrt{13})$-*R*33.7° reconstructed surface. This material is available free of charge via the Internet at http://pubs.acs.org.

AUTHOR INFORMATION

Corresponding Authors

HAMADA.Ikutaro@nims.go.jp
hitosugi@wpi-aimr.tohoku.ac.jp

Author Contributions

¶I.H. and R.S. contributed equally to this work.

Notes

The authors declare no competing financial interest.

ACKNOWLEDGMENTS

We are grateful to Filippo Federici Canova and Alexander Shluger for their critical reading of the manuscript. This work was partly supported by a Grant-in-Aid for Scientific Research (A) from the Japanese Society for Promotion of Science (JSPS). R.S. acknowledges the financial support from JSPS. Numerical calculations were performed at the Supercomputer Center, Institute for Solid State Physics, The University of Tokyo, and at the Information Technology Center, The University of Tokyo. Advanced Institute for Materials Research was established by World Premier International Research Center Initiative (WPI), MEXT, Japan. The atomic structures and STM/STS simulations were visualized by utilizing VESTA.[47]

REFERENCES

(1) Tokura, Y.; Taguchi, Y.; Okada, Y.; Fujimori, Y.; Arima, T.; Kumagai, K.; Iye, Y. *Phys. Rev. Lett.* **1993**, *70*, 2126−2129.
(2) Schooley, J. F.; Hosler, W. R.; Cohen, M. L. *Phys. Rev. Lett.* **1964**, *12*, 474−475.
(3) Müller, K. A.; Burkard, H. *Phys. Rev. B* **1973**, *19*, 3593−3602.
(4) Ohtomo, A.; Hwang, H. Y. *Nature* **2004**, *427*, 423−426.
(5) Thiel, S.; Hammerl, G.; Schmehl, A.; Schneider, C. W.; Mannhart, J. *Science* **2006**, *313*, 1942−1945.
(6) Cen, C.; Thiel, S.; Hammerl, G.; Schneider, C. W.; Andersen, K. E.; Hellberg, C. S.; Mannhart, J.; Levy, J. *Nat. Mater.* **2008**, *7*, 298−302.
(7) Reyren, N.; Thiel, S.; Caviglia, A. D.; Kourkoutis, L. F.; Hammerl, G.; Richter, C.; Schneider, C. W.; Kopp, T.; Rüetschi, A.-S.; Jaccard, D.; Gabay, M.; Muller, D. A.; Triscone, J.-M.; Mannhart, J. *Science* **2007**, *317*, 1196−1199.
(8) Brinkman, A.; Huijben, M.; van Zalk, M.; Huijben, J.; Zeitler, U.; Maan, J. C.; van der Wiel, W. G.; Rijnders, G.; Blank, D. H. A.; Hilgenkamp, H. *Nat. Mater.* **2007**, *6*, 493−496.
(9) Mavroides, J. G.; Kafalas, J. A.; Kolesar, D. F. *Appl. Phys. Lett.* **1976**, *28*, 241−243.
(10) Kudo, A.; Miseki, Y. *Chem. Soc. Rev.* **2009**, *38*, 253−278.
(11) Meevasana, W.; King, P. D. C.; He, R. H.; Mo, S.-K.; Hashimoto, M.; Tamai, A.; Songsiriritthigul, P.; Baumberger, F.; Shen, Z.-X. *Nat. Mater.* **2011**, *10*, 114−118.
(12) Santander-Syro, A. F.; Copie, O.; Kondo, T.; Fortuna, F.; Pailhès, S.; Weht, R.; Qiu, X. G.; Bertran, F.; Nicolaou, A.; Taleb-Ibrahimi, A.; Le Fèvre, P.; Herranz, G.; Bibes, M.; Reyren, N.; Apertet, Y.; Lecoeur, P.; Barthélémy, A.; Rozenberg, M. J. *Nature* **2011**, *469*, 189−193.
(13) Shimizu, R.; Iwaya, K.; Ohsawa, T.; Shiraki, S.; Hasegawa, T.; Hashizume, T.; Hitosugi, T. *ACS Nano* **2011**, *5*, 7967−7971.
(14) Kawasaki, M.; Takahashi, K.; Maeda, T.; Tsuchiya, R.; Shinohara, M.; Ishiyama, O.; Yonezawa, T.; Yoshimoto, M.; Koinuma, H. *Science* **1994**, *266*, 1540−1542.
(15) Larsen, P. K.; Dobson, P. J., Eds. *Reflection high-energy electron diffraction and reflection electron imaging of surfaces*; Plenum Press: New York, 1988.
(16) Wang, Z. L. *Reflection electron microscopy and spectroscopy for surface analysis*; Cambridge University Press: New York, 1996.
(17) Ichimiya, A.; Cohen, P. I. *Reflection high-energy electron diffraction*; Cambridge University Press: Cambridge, 2004.
(18) Kienzle, D. M.; Marks, L. D. *CrystEngComm* **2012**, *14*, 7833−7839.
(19) Shimizu, R.; Iwaya, K.; Ohsawa, T.; Shiraki, S.; Hasegawa, T.; Hashizume, T.; Hitosugi, T. *Appl. Phys. Lett.* **2012**, *100*, 263106.
(20) Naito, M.; Sato, H. *Phys. C* **1994**, *229*, 1−11.
(21) Kienzle, D. M.; Becerra-Toledo, A. E.; Marks, L. D. *Phys. Rev. Lett.* **2011**, *106*, 176102.
(22) Erdman, N.; Poeppelmeier, K. R.; Asta, M.; Warschkow, O.; Ellis, D. E.; Marks, L. D. *Nature* **2002**, *419*, 55−58.
(23) Kubo, T.; Nozoye, H. *Phys. Rev. Lett.* **2001**, *86*, 1801−1804.
(24) Johnston, K.; Castell, M. R.; Paxton, A. T.; Finnis, M. W. *Phys. Rev. B* **2004**, *70*, 085415.
(25) Lanier, C. H.; van de Walle, A.; Erdman, N.; Landree, E.; Warschkow, O.; Kazimirov, A.; Poeppelmeier, K. R.; Zegenhagen, J.; Asta, M.; Marks, L. D. *Phys. Rev. B* **2007**, *76*, 045421.
(26) Marshall, M. S. J.; Becerra-Toledo, A. E.; Marks, L. D.; Castell, M. R. *Phys. Rev. Lett.* **2011**, *107*, 086102.
(27) Becerra-Toledo, A. E.; Marshall, M. S. J.; Castell, M. R.; Marks, L. D. *J. Chem. Phys.* **2012**, *136*, 214701.

(28) Enterkin, J. A.; Subramanian, A. K.; Russell, B. C.; Castell, M. R.; Poeppelmeier, K. R.; Marks, L. D. *Nat. Mater.* **2010**, *9*, 245−248.
(29) Li, L.; Richter, C.; Mannhart, J.; Ashoori, R. C. *Nat. Phys.* **2011**, *7*, 762−766.
(30) Iwaya, K.; Shimizu, R.; Hashizume, T.; Hitosugi, T. *Rev. Sci. Instrum.* **2011**, *82*, 083702.
(31) Vanderbilt, D. *Phys. Rev. B* **1990**, *41*, 7892−7895.
(32) Wu, Z.; Cohen, R. E. *Phys. Rev. B* **2006**, *73*, 235116.
(33) Morikawa, Y.; Ishii, H.; Seki, K. *Phys. Rev. B* **2004**, *69*, 041403(R).
(34) Hellwege, K. H., Hellwege, A. M., Eds. *Ferroelectrics and Related Substances, Landolt-Börnstein, New Series Group III*; Springer-Verlag: Berlin, 1969; Vol. 3.
(35) Schmidbauer, M.; Kwasniewski, A.; Schwarzkopf, J. *J. Acta Cryst. B* **2012**, *68*, 8−14.
(36) Hamada, I.; Otani, M.; Sugino, O.; Morikawa, Y. *Phys. Rev. B* **2009**, *80*, 165411.
(37) Otani, M.; Sugino, O. *Phys. Rev. B* **2006**, *73*, 115407.
(38) Tersoff, J.; Hamann, D. R. *Phys. Rev. Lett.* **1983**, *50*, 1998−2001.
(39) Kim, M. S.; Park, C. H. *J. Korean Phys. Soc.* **2010**, *56*, 490−493.
(40) Hamann, D. R.; Vanderbilt, D. *Phys. Rev. B* **2009**, *79*, 045109.
(41) Ohsawa, T.; Shimizu, R.; Iwaya, K.; Hitosugi, T. *ACS Nano* **2014**, *8*, 2223−2229.
(42) Woolcot, T.; Teobaldi, G.; Pang, C. L.; Beglitis, N. S.; Fisher, A. J.; Hofer, W. A.; Thornton, G. *Phys. Rev. Lett.* **2012**, *109*, 156105.
(43) Salluzzo, M.; Cezar, J. C.; Brookers, N. B.; Bisogni, V.; De Luca, G. M.; Richter, C.; Thiel, S.; Mannhart, J.; Huijben, M.; Brinkman, A.; Rijnders, G.; Ghiringhelli, G. *Phys. Rev. Lett.* **2009**, *102*, 166804.
(44) Delugas, P.; Filippetti, A.; Fiorentini, V.; Bilc, D. I.; Fontaine, D.; Ghosez, Ph. *Phys. Rev. Lett.* **2011**, *106*, 166807.
(45) Lee, J.-S.; Xie, Y. W.; Sato, H. K.; Bell, C.; Hikita, Y.; Hwang, H. Y.; Kao, C.-C. *Nat. Mater.* **2013**, *12*, 703−706.
(46) Setvín, M.; Aschauer, U.; Scheiber, P.; Li, Y.-F.; Hou, W.; Schmid, M.; Selloni, A.; Diebold, U. *Science* **2013**, *341*, 988−991.
(47) Momma, K.; Izumi, F. *J. Appl. Crystallogr.* **2011**, *44*, 1272−1276.